Available online at www.sciencedirect.com

ScienceDirect

journal homepage: www.elsevier.com/locate/he

Dehydrogenation of lithium hydrazinidoborane: Insight from computational analysis

CrossMark

Tahamida Banu, Kaushik Sen, Tamalika Ash, Abhijit K. Das[*]

Department of Spectroscopy, Indian Association for the Cultivation of Science, Jadavpur, Kolkata 700032, India

ABSTRACT

Using the first-principles density functional theory approach, a detailed gas phase dehydrogenation analysis has been carried out for the monomeric as well as the dimeric units of lithium hydrazinidoborane ($LiN_2H_3BH_3$). Atoms in molecules formalism (AIM) has been employed in order to get bonding features along the desired reaction pathways. The exploration of potential energy surfaces from different structural isomers of both monomeric and dimeric hydrazinidoborane (LiHB) suggests that all the dehydrogenation reactions are endothermic in nature. Hydrogen generation from the dimeric lithium hydrazinidoborane provides an idea about the effect of neighbouring molecules on the dehydrogenation process occurring in the solid state. The lithium ion plays the central role in transferring the hydride in the dehydrogenation of both the monomeric and dimeric form of hydrazinidoborane. In summary our theoretical calculations are expected to shed light on the decomposition mechanism of alkali metal substituted hydrazine-borane type of compounds.

© 2016 Hydrogen Energy Publications LLC. Published by Elsevier Ltd. All rights reserved.

Introduction

Due to the coexistence of protic and hydridic hydrogen atoms in the same molecule, compounds having B and N entities have drawn much attention towards chemical hydrogen storage. The simplest amine-borane i.e. NH_3BH_3 (AB) provides 19.6 wt% of hydrogen storage and is proved to be one of the high-capacity solid-state based chemical hydrogen storage materials (HSM) [1,2]. Among the various approaches undertaken, modification of the chemical environment of AB through the replacement of one of its H by strongly electropositive metals (Li, Na, K) has been studied widely in order to get improved dehydrogenation properties of AB [3—17].

Hydrazine-borane ($N_2H_4BH_3$, HB), which is known to be an amino substituted derivative of AB, contains a significant amount of hydrogen content (15.4 wt%) due to the presence of four protic and three hydridic hydrogens. Discovered in the mid twentieth century and known since that time, this amine-borane derivative has recently been evaluated as an effective chemical HSM by both experimental and theoretical approaches [18,19]. However, upon heating, HB gets dehydrogenated along with the formation of toxic N_2H_4 and gaseous NH_3 in an exothermic procedure. In addition to the catalytic hydrolysis of HB [20—22], chemical modification by alkali metals (M = Li, Na, K) to form metal hydrazinidoborane ($M-N_2H_3BH_3$) is a possible pathway to facilitate effective hydrogen release from HB [23—26]. The interaction between strong Lewis base H^- of LiH with one of the protic hydrogens on the middle NH_2 group of the hydrazine-borane leads to the formation of lithium hydrazinidoborane ($LiN_2H_3BH_3$). This modification causes a strong electronic change in the $[N_2H_3BH_3]^-$ moiety and consequently an improved thermal dehydrogenation of $LiN_2H_3BH_3$. An equimolar mixture of

---

LiH—$N_2H_4BH_3$ was found to dehydrogenate more rapidly with respect to that of neat $N_2H_4BH_3$ at 150 °C [27]. Wu et al. synthesized $LiN_2H_3BH_3$ and $LiN_2H_3BH_3 \cdot 2N_2H_4BH_3$ in a ball-milling process between LiH and HB in the molar ratio of 1:1 and 1:3 respectively and showed that these materials exhibit a much higher extent of dehydrogenation, release of minimum toxic gas (i.e. NH_3, N_2H_4), and faster kinetics than pure HB [23]. Later Moury et al. synthesized the Na derivative of hydrazinidoborane (NaHB) by ball-milling process at a subsequently low temperature [24]. Moury et al., in their another work, characterized lithium hydrazinidoborane (LiHB) as a polymorphic material, with a stable low-temperature β-phase and a metastable high-temperature α-phase [26]. They also showed that after a phase transition from β- to α-LiHB, it gets dehydrogenated at a temperature 150 °C with a generation of 10 wt% of H_2 along with some polymeric residues. On the other hand, Chua et al. determined the crystal structures of NaHB and KHB and studied their dehydrogenation properties [25]. During dehydrogenation, these hydrazinidoboranes give rise to the intermediates that possess N_2BH_2, N_2BH and NBH_3 species. They also concluded that the alkali metal substituted hydrazidotrihydridoborates exhibit significantly improved dehydrogenation behaviour over pristine $N_2H_4BH_3$ with no N_2H_4 emission and greatly suppressed NH_3 release.

Although the dehydrogenation mechanism of the polymeric lithium hydrazinidoborane has been explored experimentally, there is a serious need for theoretical investigation on it to obtain fundamental insight into the reaction features. In our present study we aim to explore the formation of monomeric LiHB and its subsequent possible dehydrogenation pathways in the gas phase. In order to get a more vivid picture about the reaction occurring in the solid state, we have also studied the dehydrogenation reaction properties of its dimeric form $(LiN_2H_3BH_3)_2$. We hope that this study helps in getting a molecular level understanding of the dehydrogenation reaction mechanism of the metal hydrazinidoborane type of compounds.

Computational details

All first-principles density functional theoretical calculations are performed using Gaussian09 suite of quantum chemistry program [28]. The equilibrium geometries of all the molecular species i.e. the reactants, transition states, intermediates and products, involved in this study are optimized at the DFT level with the global hybrid meta-GGA M06-2X functional in conjunction with 6-311++G(d,p) basis set with diffuse and polarization functions. The optimized geometries along with the geometrical parameters of all the structures involved in unimolecular decomposition reactions are provided in the Supporting Information. Developed by Zhao and Truhlar [29], M06-2X functional is reported to be one of the best for studying main-group thermochemistry, kinetics and non-covalent interactions. The connecting first-order saddle points that are the transition states between the equilibrium geometries are obtained using synchronous transit-guided quasi-Newton (STQN) method. Harmonic vibrational frequencies are determined at the same M06-2X/6-311++G(d,p) level to confirm whether the optimized structures are local minima or transition states on the potential energy surfaces (PESs) and to evaluate the zero-point vibrational energy (ZPVE). The ab initio MP2 (second order Møller-Plesset perturbation theory) [30—32], along with the aug-cc-pVTZ basis set is used for single-point calculations on the M06-2X/6-311++G(d,p) optimized geometries to obtain accurate electronic energies. Parallel intrinsic reaction coordinate (IRC) [33,34], calculations are performed with all transition states to confirm whether these transition states connect the right minima or not. The potential energy surfaces (PESs) have been constructed overall using MP2/aug-cc-pVTZ//M06-2X/6-311++G(d,p) relative energies.

In order to visualize the electronic changes occurring on some important H_2 elimination pathways, atoms in molecules formalism is employed using AIMAll program [35]. Charges

(a)

(b)
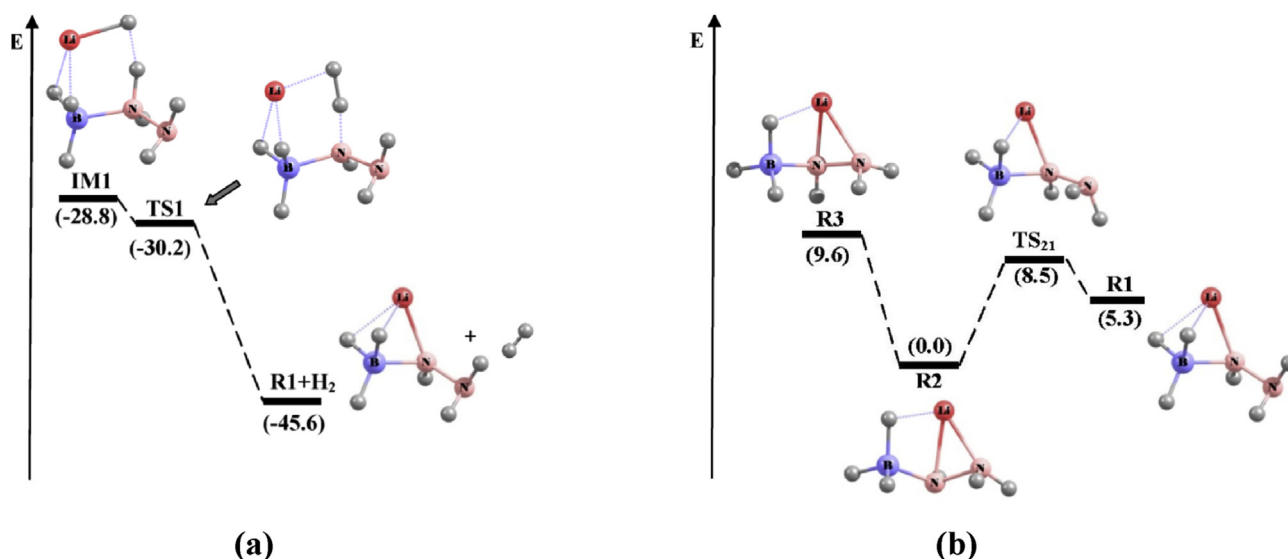
Fig. 1 — **(a) Formation of $LiN_2H_3BH_3$ (R1) and (b) its subsequent isomerization. Relative energies are in kcal/mol unit.**

are calculated at M06-2X level by applying natural population analysis.

Results and discussion

Formation of $LiN_2H_3BH_3$ and its isomerization

Fig. 1(a) summarizes the schematic potential energy surface for the formation of $LiN_2H_3BH_3$ (R1). As proposed by Chua et al. [25], the formation of alkali metal hydrazinidoborane ($MN_2H_3BH_3$, M = Li, Na, K) is highly exothermic in nature. Our study also supports this conclusion as the overall reaction's exothermicity is calculated to be −45.6 kcal/mol with respect to the reactants HB + LiH and the reaction occurs in a spontaneous way. Similar to the formation of $LiNH_2BH_3$ [12,14], here also the formation of R1 occurs due to the interaction between $H^{\delta-}$ of LiH and the $H^{\delta+}$ on internal N of HB, leading to the formation of molecular hydrogen. Consequently an ionic bond is formed between the lithium and the nitrogen atom in

the resulting dehydrogenated product (LiHB, R1). TS1 is found to be an early transition state due to its close structural similarity with the reactant-complex IM1 and at the MP2/aug-cc-pVTZ//M06-2X/6-311++G(d,p) level we predict the energy of TS1 to be 1.4 kcal/mol lower than IM1.

As shown in Fig. 1(b), the formed hydrazinidoborane R1 undergoes isomerization through TS21 and generates its more stable isomer R2. Energetically R2 is found to be 5.3 kcal/mol lower than R1. The lithium which is attached to the internal N in R1 isomer migrates to the terminal N in R2. Situated at an energy level of 9.6 kcal/mol relative to R2, another isomer R3, on the other hand, generates R2 through a barrier less fashion. R2 and R3 differ in the angle of orientation of the H atom attached to the internal N of the system. As the energy ordering dictates, R2 is the most stable isomer of LiHB, followed by R1 and R3 isomers.

Decomposition of R1 isomer

Decomposition of R1 proceeds through two different pathways, pathway 1 and pathway 2, respectively.
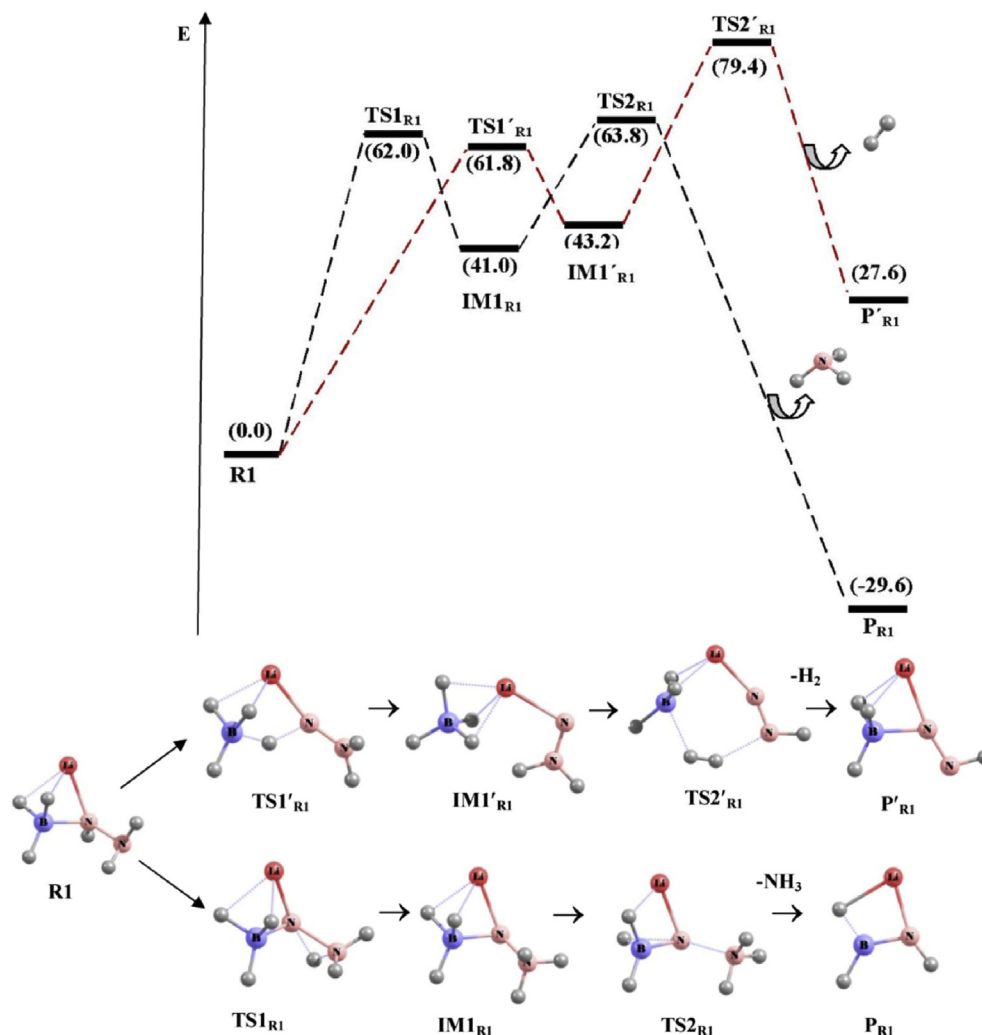
Fig. 2 — Decomposition channels of R1 isomer of $LiN_2H_3BH_3$ represented by both potential energy surface and schematic diagrams. The pathway 1 and pathway 2 are denoted by black and red dashed lines respectively. Relative energies are in kcal/mol unit. (For interpretation of the references to colour in this figure legend, the reader is referred to the web version of this article.)

Pathway 1

As evident from the PES in Fig. 2, the reactant R1 leads to the intermediate IM1$_{R1}$, through the transition state TS1$_{R1}$. TS1$_{R1}$ is found to be 62.0 kcal/mol higher in energy relative to the reactant and involves 1,2 H-shift across the N−N bond. The intermediate IM1$_{R1}$, in the next step, gets dissociated into P$_{R1}$ and molecular NH$_3$ through the transition state TS2$_{R1}$ and this process is associated with an activation barrier of 22.8 kcal/mol. The breaking of bond between two N atoms and 1,2-shift of H across the B−N bond occurs simultaneously in TS2$_{R1}$. This overall two-step NH$_3$ release channel is calculated to be highly exothermic in nature.

Pathway 2

As depicted in Fig. 2, pathway 2 happens to be a two-step reaction similar to pathway 1. The first step involves the formation of an isomer IM1'$_{R1}$ which is situated at a well depth of 43.2 kcal/mol relative to R1. This step passes through an energy barrier of 61.8 kcal/mol and in the accompanying transition state, TS1'$_{R1}$, 1,2-H-shift occurs across the B−N bond along with intramolecular B−N bond dissociation; the distance between B and N being 2.524 Å. In the following step, H$_2$ abstraction takes place from IM1'$_{R1}$ via the formation of a five-member transition state TS2'$_{R1}$. The B−N bond is reformed simultaneously in this step. This connecting TS is situated at
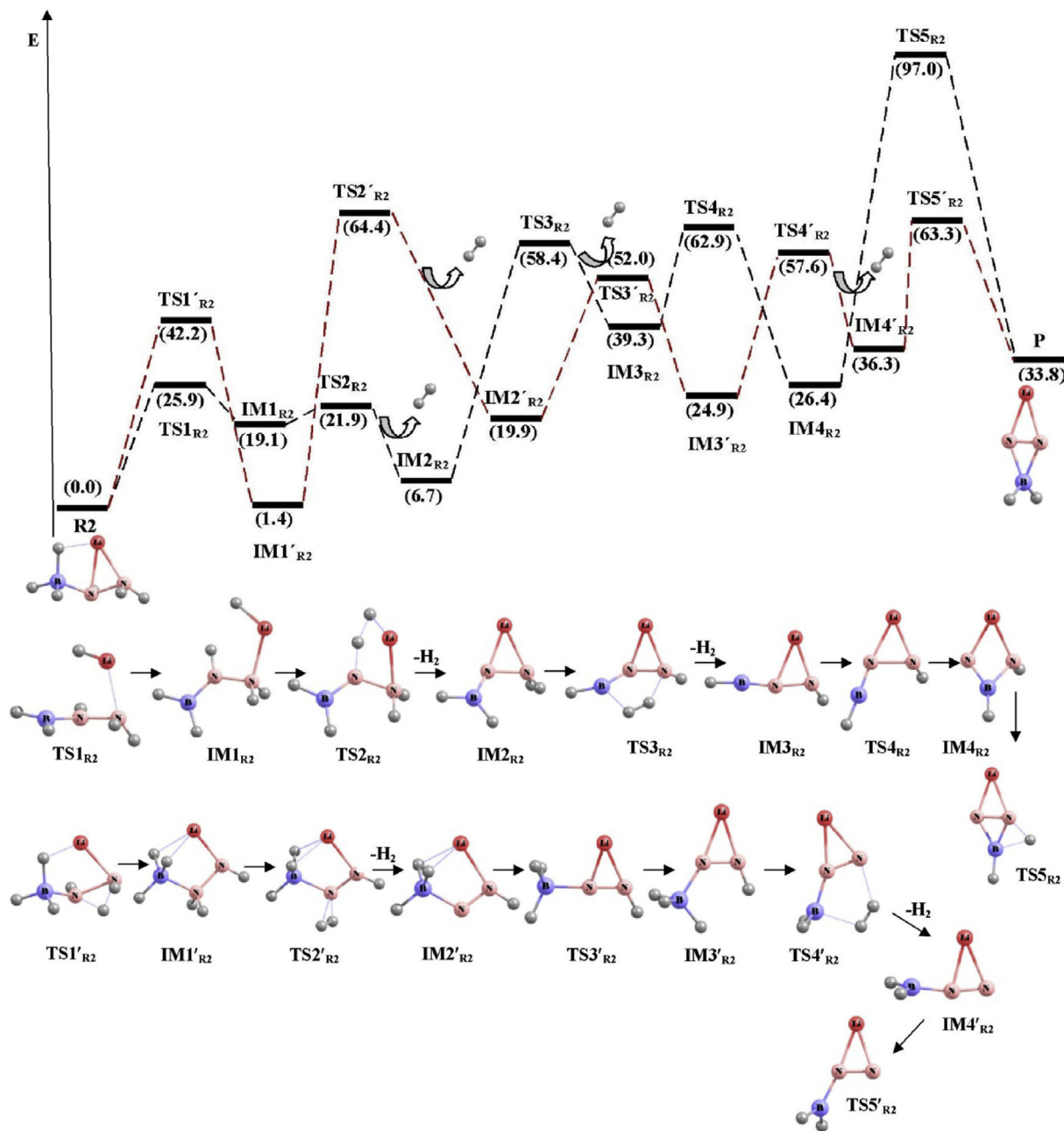
Fig. 3 − Decomposition channels of R2 isomer of LiN$_2$H$_3$BH$_3$, represented by both potential energy surface and schematic diagrams. The pathway 1 and pathway 2 are denoted by black and red dashed lines respectively. Relative energies are in kcal/mol unit. (For interpretation of the references to colour in this figure legend, the reader is referred to the web version of this article.)

an energy level of 36.2 kcal/mol with respect to the intermediate $IM1'_{R1}$. The two departing hydrogen atoms in the H-bridge of $TS2'_{R1}$ interact with each other at a distance 0.778 Å, leading to the formation of molecular H_2 and the product P'_{R1}.

Decomposition of R2

Similar to R1, R2 is also found to decompose through two different pathways and this is displayed in Fig. 3.

Pathway 1
In the first step of this dehydrogenation pathway, lithium of R2 abstracts a hydride from B and forms an intermediate $IM1_{R2}$. The transition state, $TS1_{R1}$, located for this conversion, is situated at an energy level of 25.9 kcal/mol relative to R2. In the subsequent step, interaction between Li—H complex and the protic H attached to the central N in the intermediate $IM1_{R2}$ leads to the generation of $IM2_{R2}$ along with the

molecular hydrogen. Our result finds support from the experimental observation by Chua et al. [25], where they suggested that the light alkali metal acts as a hydrogen carrier and by forming M-H complex it combines with the protic hydrogen to form molecular hydrogen. The corresponding transition state for this step, $TS2_{R2}$, involves formation of a five-member ring in which the two departing H-atoms interact with each other at a distance of 1.074 Å. $IM2_{R2}$ further gets dehydrogenated in the next step via the formation of a five-member transition state $TS3_{R2}$. The distance between the two departing H atoms in $TS3_{R2}$ is calculated to be 0.851 Å. It is evident from the PES in Fig. 3 that the formed product undergoes isomerization and generates its final isomer P via two transition states $TS4_{R2}$ and $TS5_{R2}$ with activation barriers of 23.6 kcal/mol and 70.6 kcal/mol respectively. It should be noted here that all the dehydrogenation pathways originating from R2 and R3 are found to lead to the same common end product, P.
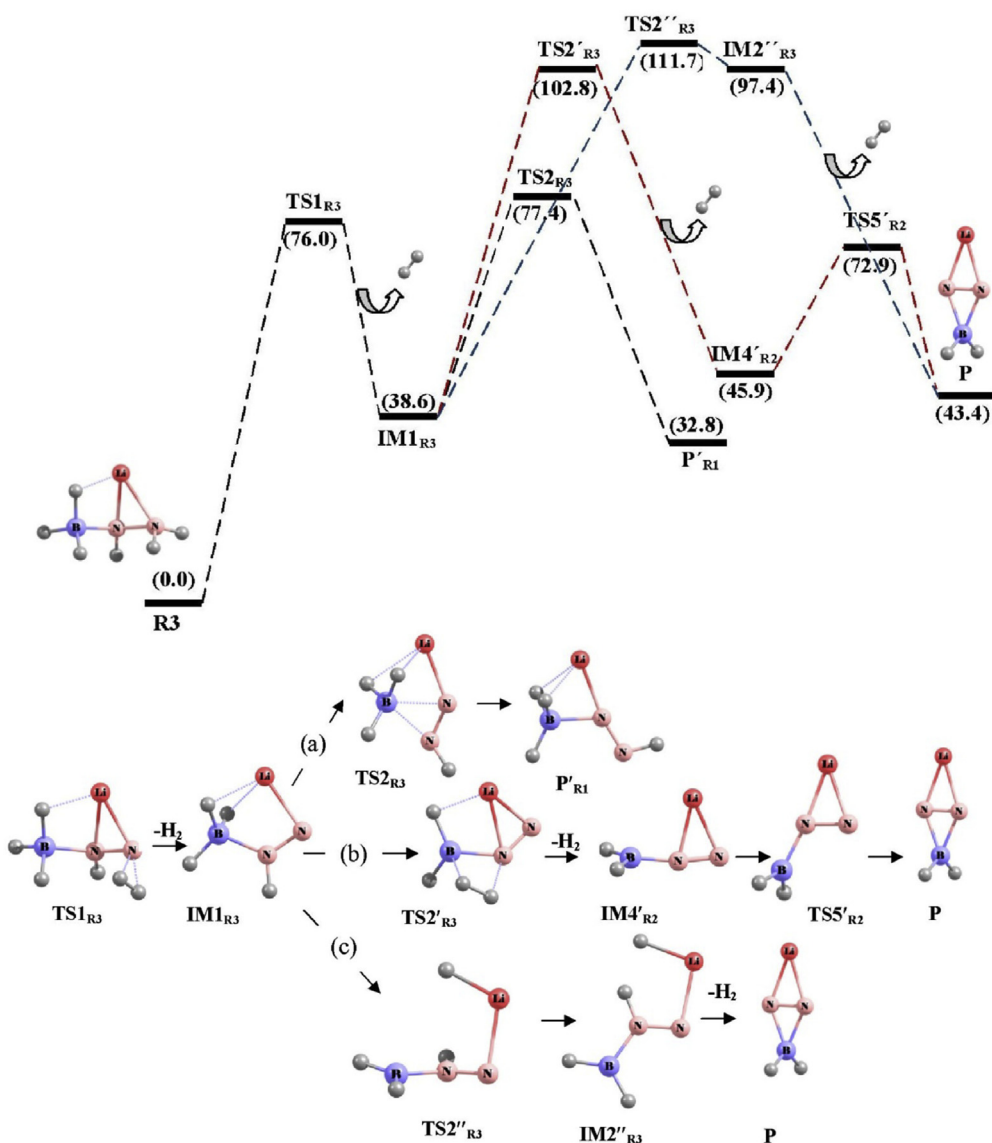
Fig. 4 — Decomposition channels of R3 isomer of $LiN_2H_3BH_3$ (pathway 1), represented by both potential energy surface and schematic diagrams. Relative energies are in kcal/mol unit.

Pathway 2

Pathway 2 starts with an intramolecular H atom transfer be-tween the two nitrogen atoms in the transition state $TS1'_{R2}$. This transfer leads to the formation of an intermediate $IM1'_{R2}$ and the energy barrier associated with this conversion is calculated to be 42.2 kcal/mol. The two hydrogen atoms, attached to the internal N in $IM1'_{R2}$, depart together in the next step by forming a bond between them and this occurs through the formation the transition state $TS2'_{R2}$ (1515.6i cm^{-1}).

In order to get insight into the evolution of bonding during the course of this dehydrogenation step, we have employed bonding evolution theory (BET) using AIM formalism. While the topological properties of the charge density at bond critical points (BCPs) associated with this dehydrogenation mecha-nism are given in Table S1 in the supplementary material, the important molecular graphs along with the reaction pathway are depicted in Fig. S2. As apparent from the molecular graphs in Fig. S2, one of the hydrogens from the internal N first gets detached from the system as a hydride. The driving force behind this is the presence of the neighbouring N that helps detaching the hydride by donating its lone pair of electrons to the N−N bond, which results in the formation of double bond between these two nitrogens. Consequently another H, attached to the internal N, departs as a proton by interacting with the hydride at a distance 1.101 Å in $TS2'_{R2}$ and together they form a H$_2$ molecule. This rationalization is also supported by the charges accumulated by these two H atoms in $TS2'_{R2}$, which are calculated to be −0.038 a.u. and +0.348 a.u. respectively. The corresponding energy barrier associated with this dehydrogenation process is calculated to be 63.0 kcal/mol relative to $IM1'_{R2}$. This step gives rise to the formation of $IM2'_{R2}$ + H$_2$ which is energetically 19.9 kcal/mol higher with respect to the reactant R2. The intermediate $IM2'_{R2}$, thus formed, undergoes isomerization in the next step and leads to the generation of another isomer $IM3'_{R2}$ via the transition state $TS3'_{R2}$. This is followed by the H$_2$-elimination

from $IM3'_{R2}$ in the next step leading to the formation of $IM4'_{R2}$, via the transition state $TS4'_{R2}$. This transition state, charac-terized by a five-member ring, is 32.7 kcal/mol higher in en-ergy than $IM3'_{R2}$, and holds a H−H distance of 0.824 Å. The intermediate $IM4'_{R2}$ further isomerizes to form the final product P through the transition state $TS5'_{R2}$ with an energy barrier of 27.0 kcal/mol.

Decomposition of R3 isomer

Again, the decomposition of R3 isomer is found to proceed through two different pathways, as depicted in Figs. 4 and 5 respectively.

Pathway 1

As can be seen from the PES in Fig. 4, this decomposition pathway, originating from R3 is a complex one. The reactant R3 first gives rise to the formation of the intermediate $IM1_{R3}$, passing through the transition state $TS1_{R3}$ (1377.3i cm^{-1}). Similar to $TS2'_{R2}$, here also the two H atoms get departed from the same N atom (terminal one) and together they form a H$_2$ molecule. From the molecular graphs along this reaction pathway (Fig. S3), and the $\nabla^2\rho$ values at the H−H BCP (Table S2) involved in the dehydrogenation mechanism, it can be observed that the bond between these two departing H atoms has already been initiated before reaching the $TS1_{R3}$, where the two H atoms hold a distance of 0.862 Å and the corre-sponding electronic charges accumulated by these H atoms are calculated to be +0.167 a.u and +0.199 a.u. respectively.

$IM1_{R3}$, subsequently, leads to the generation of three different reaction channels, (a), (b) and (c) respectively. While channel (a) is an isomerization pathway, the other two channels are found to be the dehydrogenation ones. Through channel (a), $IM1_{R3}$ is converted to its isomer P'_{R1} and the pro-cess is associated with an activation barrier of 38.8 kcal/mol. It should be noted here that the same product P'_{R1} is also found
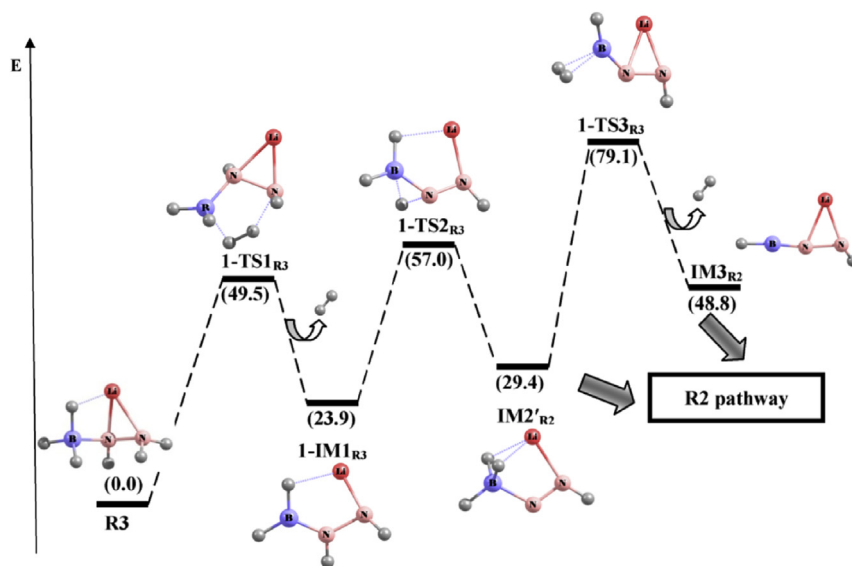
Fig. 5 − Decomposition channels of R3 isomer of LiN$_2$H$_3$BH$_3$ (pathway 2), represented by both potential energy surface and schematic diagrams. Relative energies are in kcal/mol unit.

to be generated in the previously discussed R1 decomposition channel. IM1$_{R3}$, in channel (b), passes through the transition state TS2′$_{R3}$ and forms IM4′$_{R2}$ through H$_2$-elimination. IM4′$_{R2}$ finally leads to the formation of product P following the same decomposition channel as that of R2. Now, considering the (c) pathway, IM1$_{R3}$ is found to give rise to a relatively high energy intermediate IM2″$_{R3}$ traversing a very high energy barrier of 73.1 kcal/mol. In spite of our numerous attempts, we were unable to locate any transition state for the H$_2$ loss from IM2″$_{R3}$, which finally leads to the product P with an energy loss of 54.0 kcal/mol.

Pathway 2

Starting from the reactant R3, this decomposition pathway passes through the transition state 1-TS1$_{R3}$ and requires a considerably high energy barrier of 49.5 kcal/mol. This TS consists of a five-member ring in which the two departing H atoms interact with each other at a distance 0.879 Å. The

intermediate 1-IM1$_{R3}$, so formed, undergoes isomerization in the next step with an energy barrier of 33.1 kcal/mol and enters the R2 decomposition channel by forming IM2′$_{R2}$. The associated transition state, 1-TS2$_{R3}$, for this step, exhibits an intramolecular 1,2-H-shift along the B−N bond. In an ensuing dehydrogenation in the next step, the two hydrogen atoms attached to B in IM2′$_{R2}$ departs together as H$_2$ molecule along with the formation of intermediate IM3$_{R2}$ and thereafter the intermediate enters the R2 decomposition pathway. The distance between these two departing H atoms are found to be 0.789 Å in the corresponding transition state 1-TS3$_{R3}$, which is almost nearer to the actual H$_2$ bond length. As dictated by the molecular graphs in Fig. S4, $\nabla^2\rho$ values at H−H BCP (Table S3), as well as the charges on these H atoms (+0.106 a.u., +0.098 a.u.), H$_2$ molecule formation is expected to be initiated long before the attainment of the corresponding TS, 1-TS3$_{R3}$.
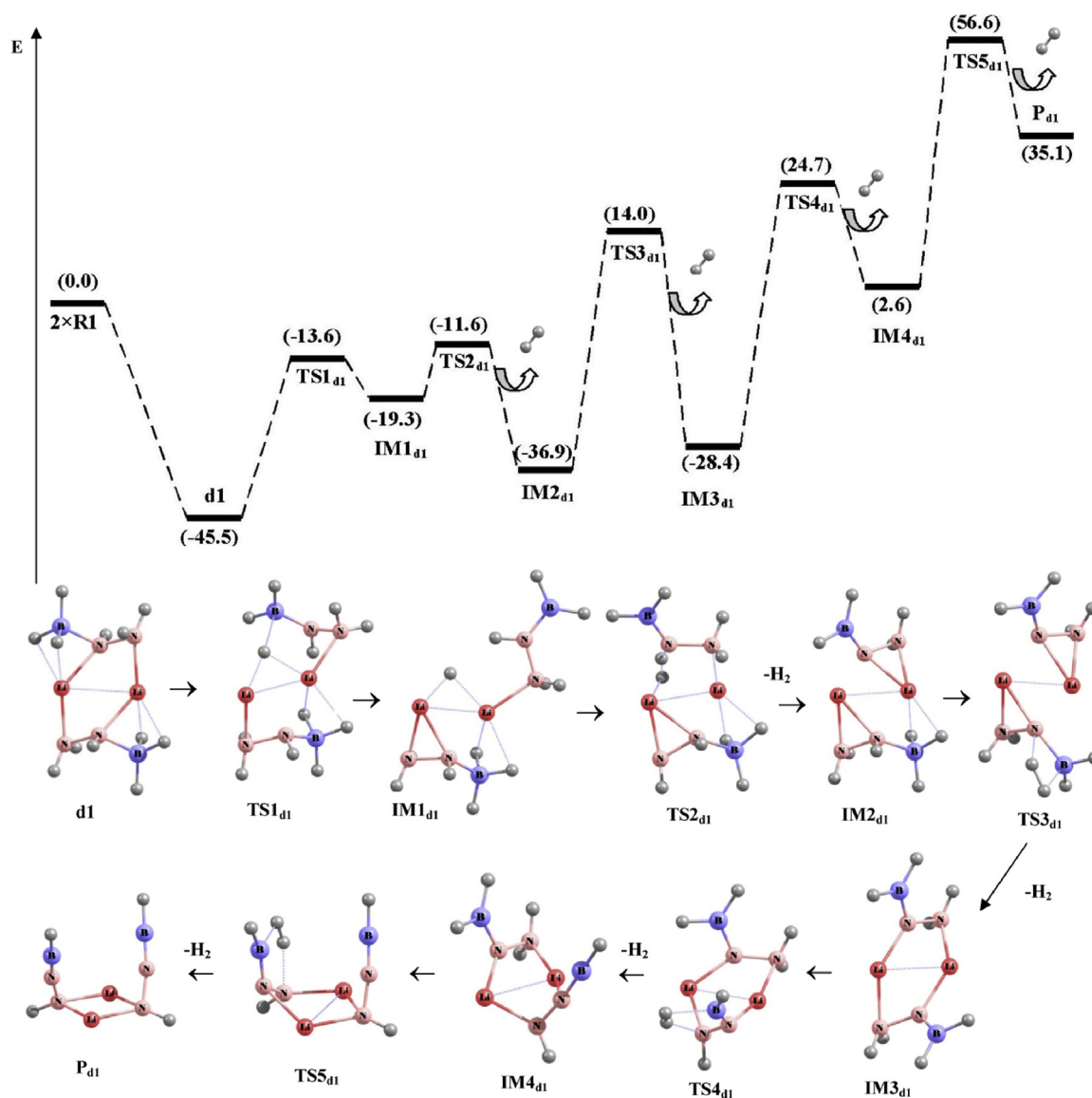
Fig. 6 − Dehydrogenation pathway of d1 dimer, represented by both potential energy surface and schematic diagrams. Relative energies are in kcal/mol unit.

Pathways for H₂ release from dimer (LiN₂H₃BH₃)₂

As the interaction between the two monomeric units of LiN₂H₃BH₃ may lead to lower energy pathways, we have considered the possible reaction pathways generated from the dimer and constructed the corresponding potential energy surfaces (PESs) depicted in Figs. 6 and 7 respectively. We have found the two stable dimers of LiN₂H₃BH₃ namely d1 and d2 respectively. The dimer d2 has complexation energy of −16.6 kcal/mol and is formed mainly due to the interaction of one lithium of one monomer with the two Hs attached to boron of other monomer. On the other hand, dimer d1 is found to be more stable due to its more negative complexation energy (−45.5 kcal/mol) compared to dimer d2. Lithium of each

monomeric unit in dimer d1 interacts with the nitrogen of another monomer, thereby forming a stable ring structure with the N backbones and the two lithium atoms. It is noteworthy that the monomeric unit present in these two dimers is R1. The possible H₂ release pathways from these two isomers are detailed in the following section.

H₂ release pathway from dimer d1

Having formed, the dimer d1 undergoes dehydrogenation through a multistep reaction pathway. The first step has a relatively high energy barrier of 31.9 kcal/mol and involves the transfer of H atom from boron to lithium and render the formation of a Li_2−H triangular moiety in the resultant $IM1_{d1}$ intermediate. The corresponding transition state for this step is
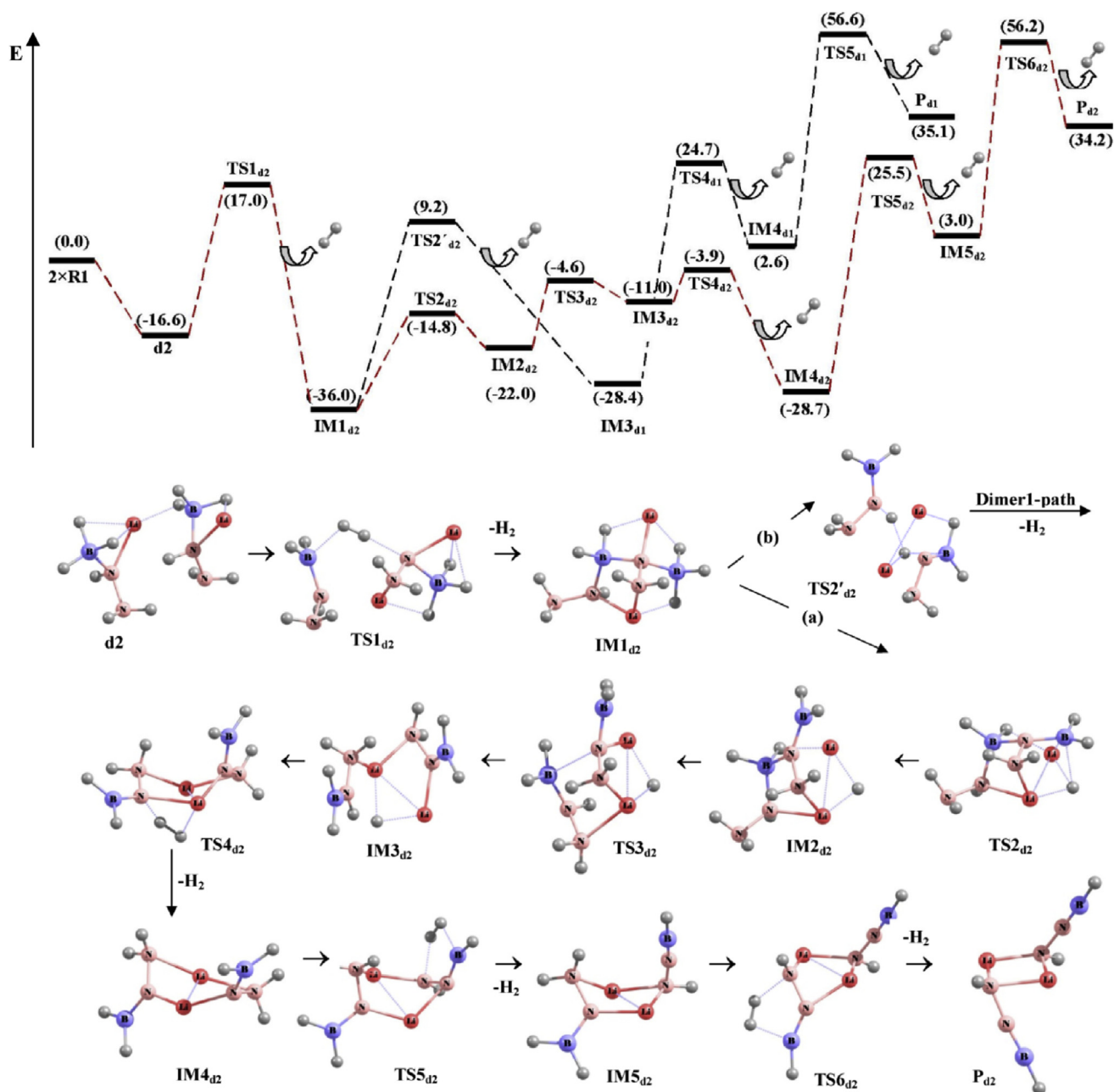
Fig. 7 − Dehydrogenation pathways of d2 dimer, represented by both potential energy surface and schematic diagrams. Relative energies are in kcal/mol unit.

TS1$_{d1}$. Associated with a small energy barrier of 7.7 kcal/mol, IM1$_{d1}$ is dehydrogenated in the next step with the formation of IM2$_{d1}$ and molecular hydrogen. The two H atoms from Li$_2$ and N moieties in the corresponding transition state TS2$_{d1}$ get departed by forming a bond between them; the distance between these two departing H atoms being 1.052 Å. IM2$_{d1}$ further rearranges to form IM3$_{d1}$ + H$_2$ via the transition state TS3$_{d1}$, in which the two H atoms from B and N depart and form molecular H$_2$ together. For this step also, the energy barrier remains considerably high (50.9 kcal/mol). The next two steps involve dehydrogenation successively via the formation of the transition states TS4$_{d1}$ and TS5$_{d1}$ with high energy barriers of 53.1 kcal/mol and 54.0 kcal/mol respectively. This pathway ends up giving the final product P$_{d1}$ along with four molecules H$_2$ with an overall reaction endothermicity of 35.1 kcal/mol.

H$_2$ release pathway from dimer d2

As apparent from the PES in Fig. 7, the dimer d2 first form IM1$_{d2}$ and molecular H$_2$ through the formation of the transition state TS1$_{d2}$ which has an energy barrier of 33.6 kcal/mol. Two different pathways get generated from the intermediate IM1$_{d2}$ and these are classified as (a) and (b) pathways respectively.

Pathway (a) proceeds through the transition state TS2$_{d2}$, situated at an energy level of 21.2 kcal/mol higher with respect to IM1$_{d2}$. This transition state involves the transfer of hydrogen atom from B to Li which leads to the formation of Li$_2$–H type of triangular moiety in the produced intermediate IM2$_{d2}$. The structure of this intermediate is entirely different from that of IM1$_{d1}$ although similar type of Li$_2$–H structure is found to be present in both of these intermediates. IM2$_{d2}$ further rearranges to form IM3$_{d2}$ through the transition state TS3$_{d2}$ in which the intermolecular B–N bond gets dissociated. Situated at a well depth of −11.0 kcal/mol with respect to the starting reactants *i.e.* 2(LiN$_2$H$_3$BH$_3$), IM3$_{d2}$ in the next step undergoes dehydrogenation via the transition state TS4$_{d2}$ in which the two H atoms from Li$_2$ moiety and N depart together and consequently make a bond between them, the distance between these two departing H atoms is calculated to be 1.046 Å. The associated energy barrier of this step is calculated to be 7.1 kcal/mol. In the following two steps, dehydrogenation occurs through the two transition states TS5$_{d2}$ and TS6$_{d2}$ respectively which are associated with considerably high energy barriers of 54.2 kcal/mol and 53.2 kcal/mol respectively. As shown in Fig. 7, the resultant product is P$_{d2}$ which is nothing but another isomer of P$_{d1}$, formed in the decomposition pathway of d1 dimer.

Originating from the intermediate IM1$_{d2}$, (b) pathway enters the dimer d1 decomposition channel after a one-step reaction. The formed TS2′$_{d2}$ involves dehydrogenation as the two H atoms from N and B makes a bond between them (1.531 Å) and are departed from the system as molecular hydrogen along with the formation of IM3$_{d1}$. At this point d2 dimer pathway converges with the dimer d1 decomposition channel which finally ends up producing the product P$_{d1}$.

Conclusion

In this work, we have systematically explored and analysed the potential energy surfaces for the decomposition of monomeric and dimeric lithium hydrazinidoborane. The three isomers of LiHB are found to be energetically close to each other and all of them undergo dehydrogenation processes which are subsequently characterized from a thermodynamic point of view. Among all the decomposition pathways from monomeric LiHB, NH$_3$ release channel, originating from R1 isomer, is found to be highly exothermic in nature. Comparison of the hydrogen elimination from all of these three isomers of LiHB shows that most of the dehydrogenation steps are energetically unfavourable due to the high energy barriers associated with them. In case of monomeric dehydrogenation channels, hydrogen generation is only found to be possible from the lower energy decomposition channel originated from R2 isomer (pathway 1). Similar to the LiNH$_2$BH$_3$, here also the lithium ion acts as a hydride transfer shuttle in a two stage dehydrogenation mechanism and helps releasing the first molecular hydrogen in a facile process with an energy barrier of 2.8 kcal/mol. On the other hand, two lithium ions together play the role of hydrogen carrier in the dehydrogenation of dimeric lithium hydrazinidoborane, via formation of the Li$_2$–H complex. The barrier for the first hydrogen release from dimer d1 is found to be 7.7 kcal/mol, while in case of dimer d2, this barrier is calculated to be energetically high (33.6 kcal/mol). Therefore, from the viewpoint of first dehydrogenation step, it can be articulated that dehydrogenation from d1 isomer is preferred over d2 isomer. By studying the dehydrogenation steps of dimeric LiHB, we can get an idea about the role of the surrounding molecules on the reaction mechanism, which actually takes place in the solid state. We expect our theoretical work, which is the first to investigate the dehydrogenation mechanism in alkali metal-hydrazinidoborane type complexes, would invite further theoretical and experimental investigations on designing better hydrogen storage materials.

Appendix A. Supplementary data

Supplementary data related to this article can be found at http://dx.doi.org/10.1016/j.ijhydene.2016.08.218.

R E F E R E N C E S

[1] Stephens FH, Pons V, Baker RT. Ammonia–borane: the hydrogen source par excellence? Dalton Trans 2007:2613–26.

[2] Marder TB. Will we soon be fueling our automobiles with ammonia–borane? Angew Chem Int Ed 2007;46:8116–8.

[3] Lu J, Fang ZZ, Sohn HY. A dehydrogenation mechanism of metal hydrides based on interactions between H$^{\delta+}$ and H$^-$. Inorg Chem 2006;45:8749–54.

[4] Xiong ZT, Yong CK, Wu G, Chen P, Shaw W, Karkamkar A, et al. High-capacity hydrogen storage in lithium and sodium amidoboranes. Nat Mater 2008;7:138–41.

[5] Kang X, Fang Z, Kong L, Cheng H, Yao X, Lu G, et al. Ammonia borane destabilized by lithium hydride: an advanced on-board hydrogen storage material. Adv Mater 2008;20:2756–9.

[6] Wu H, Zhou W, Yildirim T. Alkali and alkaline-earth metal amidoboranes: structure, crystal chemistry, and hydrogen storage properties. J Am Chem Soc 2008;130:14834–9.

[7] Xiong ZT, Chua YS, Wu GT, Xu WL, Chen P, Shaw W, et al. Interaction of lithium hydride and ammonia borane in THF. Chem Commun 2008:5595–7.

[8] Xiong ZT, Wu GT, Chua YS, Hu JJ, He T, Xu WL, et al. Synthesis of sodium amidoborane ($NaNH_2BH_3$) for hydrogen production. Energy Environ Sci 2008;1:360–3.

[9] Fijalkowski KJ, Grochala W. Substantial emission of NH_3 during thermal decomposition of sodium amidoborane, $NaNH_2BH_3$. J Mater Chem 2009;19:2043–50.

[10] Ramzan M, Silvearv F, Blomqvist A, Scheicher RH, Lebègue S, Ahuja R. Structural and energetic analysis of the hydrogen storage materials $LiNH_2BH_3$ and $NaNH_2BH_3$ from ab initio calculations. Phys Rev B Condens Matter Mater Phys 2009;79. 132102.

[11] Lee TB, Mckee ML. Mechanistic study of $LiNH_2BH_3$ formation from $(LiH)_4 + NH_3BH_3$ and subsequent dehydrogenation. Inorg Chem 2009;48:7564–75.

[12] Kim DY, Singh NJ, Lee HM, Kim KS. Hydrogen-release mechanisms in lithium amidoboranes. Chem Eur J 2009;15:5598–604.

[13] Kim DY, Lee HM, Seo J, Shin SK, Kim KS. Rules and trends of metal cation driven hydride-transfer mechanisms in metal amidoboranes. Phys Chem Chem Phys 2010;12:5446–53.

[14] Swinnen S, Nguyen VS, Nguyen MT. Potential hydrogen storage of lithium amidoboranes and derivatives. Chem Phys Lett 2010;489:148–53.

[15] Staubitz A, Robertson APM, Manners I. Ammonia-borane and related compounds as dihydrogen sources. Chem Rev 2010;110:4079–124.

[16] Chua YS, Chen P, Wu G, Xiong Z. Development of amidoboranes for hydrogen storage. Chem Commun 2011;47:5116–29.

[17] Shevlin SA, Kerkeni B, Guo ZX. Dehydrogenation mechanisms and thermodynamics of MNH_2BH_3 (M = Li, Na) metal amidoboranes as predicted from first principles. Phys Chem Chem Phys 2011;13:7649–59.

[18] Goubeau J, Ricker E. Borinhydrazin und seine Pyrolyseprodukte. Z Anorg Allg Chem 1961;310:123–42.

[19] Moury R, Moussa G, Demirci UB, Hannauer J, Bernard S, Petit E, et al. Hydrazine borane: synthesis, characterization, and application prospects in chemical hydrogen storage. Phys Chem Chem Phys 2012;14:1768–77.

[20] Hannauer J, Akdim O, Demirci UB, Geantet C, Herrmann JM, Miele P, et al. High-extent dehydrogenation of hydrazine borane $N_2H_4BH_3$ by hydrolysis of BH_3 and decomposition of N_2H_4. Energy Environ Sci 2011;4:3355–8.

[21] Karahan S, Zahmakıran M, Özkar S. Catalytic hydrolysis of hydrazine borane for chemical hydrogen storage: highly efficient and fast hydrogen generation system at room temperature. Int J Hydrogen Energy 2011;36:4958–66.

[22] Çelik D, Karahan S, Zahmakıran M, Özkar S. Hydrogen generation from the hydrolysis of hydrazine-borane catalyzed by rhodium(0) nanoparticles supported on hydroxyapatite. Int J Hydrogen Energy 2012;37:5143–51.

[23] Wu Y, Zhou W, Pinkerton FE, Udovic TJ, Yildirim T, Rush JJ. Metal hydrazinoborane $LiN_2H_3BH_3$ and $LiN_2H_3BH_3 \cdot 2N_2H_4BH_3$: crystal structures and high-extent dehydrogenation. Energy Environ Sci 2012;5:7531–5.

[24] Moury R, Demirci UB, Ichikawa T, Filinchuk Y, Chiriac R, van der Lee A, et al. Sodium hydrazinidoborane: a chemical hydrogen-storage material. ChemSusChem 2013;6:667–73.

[25] Chua YS, Pei Q, Ju X, Zhou W, Udovic TJ, Wu G, et al. Alkali metal hydride modification on hydrazine borane for improved dehydrogenation. J Phys Chem C 2014;118:11244–51.

[26] Moury R, Demirci UB. Hydrazine borane and hydrazinidoboranes as chemical hydrogen storage materials. Energies 2015;8:3118–41.

[27] Hügle T, Kühnel MF, Lentz D. Hydrazine borane: a promising hydrogen storage material. J Am Chem Soc 2009;131:7444–6.

[28] Frisch MJ, Trucks GW, Schlegel HB, Scuseria GE, Robb MA, Cheeseman JR, et al. Gaussian 09, revision D.01. Wallingford, CT: Gaussian, Inc.; 2009.

[29] Zhao Y, Truhlar DG. The M06 suite of density functionals for main group thermochemistry, thermochemical kinetics, noncovalent interactions, excited states, and transition elements: two new functionals and systematic testing of four M06-class functionals and 12 other functionals. Theor Chem Acc 2008;120:215–41.

[30] Head-Gordon M, Pople JA, Frisch MJ. MP2 energy evaluation by direct methods. Chem Phys Lett 1988;153:503.

[31] Saebø S, Almlöf J. Avoiding the integral storage bottleneck in LCAO calculations of electron correlation. Chem Phys Lett 1989;154:83.

[32] Frisch MJ, Head-Gordon M, Pople JA. A direct MP2 gradient method. Chem Phys Lett 1990;166:275.

[33] Gonzalez C, Schlegel HB. An improved algorithm for reaction path following. J Chem Phys 1989;90:2154–61.

[34] Gonzalez C, Schlegel HB. Reaction path following in mass-weighted internal coordinates. J Phys Chem 1990;94:5523–7.

[35] Keith TA. AIMAll, 14.06.21. Overland Park, KS: TK Gristmill Software; 2013. http://aim.tkgristmill.com.